JPEDAV (2010) 31:341–347
DOI: 10.1007/s11669-010-9727-3
1547-7037 ©ASM International

Reuse of RO Desalination Plant Reject Brine

Ferid Hajbi, Halim Hammi, and Adel M'nif

(Submitted July 27, 2009)

In this work we try to study the feasibility of salt production from a reject brine coming from a desalination plant in Skhira in the south of Tunisia, This plant treats 22,008 m^3/day of raw water to produce 9984 m^3 of fresh water and 12,024 m^3 of rejected water and has the advantages of being environmentally friendly and producing commercial products in crystalline, slurry, and liquid forms. The process involves an application of the solubility diagrams in order to valorize the reject brines. These solutions are considered as strongly concentrated brines and containing several elements such as: Na^+, K^+, Mg^{2+}, Ca^{2+}, Cl^-, and SO_4^{2-}. This observation leads us to consider the complete hexary system Na^+, Mg^{2+}, K^+, Ca^{2+}/Cl^-, $SO_4^{2-}//H_2O$ which includes four quinary systems. A number of physico-chemical analyses were employed (Potentiometry, complexometry, gravimetry, XRD, and SEM). At the end of an isothermal and isobaric evaporation of the reject brine, we could recover various salts (NaCl, KCl, $CaSO_4{\cdot}2H_2O$, $MgSO_4{\cdot}7H_2O$…) very useful for industry and agriculture.

Keywords brines, evaporation, hexary system, reverse osmosis, solubility diagrams

1. Introduction

This paper will focus on how saline effluent resulting from desalination plants could be used as raw material on solar ponds in order to recover salts very useful for industry and agriculture.[1-6] In fact the generation of saline effluent from direct desalination or industry is viewed as severe environmental problem.[7,8] The brine disposal exhibits elevated salt contents. So this brine must be properly managed in order to avoid environmental contamination.[9,10] On the other hand, the natural evaporation could be applied to reduce the energy consumption of the treatment and the associated costs. Many authors treated these concentrated solutions as a reciprocal quinary system (class II)[11,12] Na^+, K^+, Mg^{2+}/Cl^-, $SO_4^{2-}//H_2O$, they supposed that calcium had a very low concentration and it was ignored.[13] However, in the reject brine resulting from the studied desalination plants, the calcium is abundant and must to be considered. So if we add calcium to the quinary system we obtain a hexary system with seven constituents with the electrical neutrality condition, and can be expressed in a six-component space.[14] Hence, in an NaCl-saturated Jänecke projection.

Ferid Hajbi, Halim Hammi, and **Adel M'nif**, LVRNMR, National Centre of Research in Materials Science; Technologic Park of Borj Cedria, B.P. 95-2050 Hammam-Lif, Tunisia. Contact e-mail: halim.hammi@inrst.rnrt.tn.

Mineral abbreviations

Chemical formula	Abbreviation	Mineralogical name
$3K_2SO_4{\cdot}Na_2SO_4$	Ap	Aphthialite
$CaCl_2{\cdot}6H_2O$	Ant	Antarcticite
$CaSO_4$	A	Anhydrite
$CaSO_4{\cdot}2H_2O$	G	Gypse
$K_2Ca(SO_4)_2{\cdot}6H_2O$	Syn	Syngenite
$K_2Mg(SO)_2{\cdot}4H_2O$	Le	Leonite
$K_2Mg(SO_4)_2{\cdot}6H_2O$	Pic	Picromérite
$K_2MgCa_2(SO_4)_4{\cdot}2H_2O$	Po	Polyhalite
KCl	Syl	Sylvite
$KCl{\cdot}MgSO_4{\cdot}3H_2O$	Ka	Kainite
$KMgCl_3{\cdot}6H_2O$	Car	Carnallite
$Mg_2CaCl_6{\cdot}12H_2O$	Tc	Tachyhydrite
$MgCl_2{\cdot}6H_2O$	Bi	Bishofite
$MgSO_4{\cdot}6H_2O$	Hx	Hexahydrite
$MgSO_4{\cdot}7H_2O$	Ep	Epsomite
$MgSO_4{\cdot}H_2O$	Ki	Kiéserite
$Na_2Mg(SO_4)_2{\cdot}4H_2O$	Bl	Bloedite
$Na_2Ca(SO_4)_2$	Gl	Glauberite
$Na_2SO_4{\cdot}10H_2O$	Th	Thenardite
NaCl	H	Halite

2. Description of the Desalination Unit

The station of Skhira is located near the plant of phosphoric acid (Tunisian Chemical Group). Drilling water is pumped from five wells, before entering the treatment, water is passed through a sand filter and microfilters, to eliminate all impurities and suspended solids. This unit has four main lines, three lines (A, B, and C) with cellulose acetate membranes (each line contains 28 tubes each containing four membranes). The fourth line is a pilot (D) and employs polyamide membranes (10 tubes each containing five membranes).

Table 1 Characteristics of reverse osmosis lines (Skhira station)

	Treated water volume, m^3/day	Permeate volume, m^3/day	Concentrate volume, m^3/day
Lines A, B, and C	20160	8784	11376
Line D	1848	1200	648
Total	22008	9984	12024

Table 2 Composition of raw water, permeate, and concentrate

Designation	Units	Raw water	Permeate	Concentrate
Temperature	°C	30	30	30
pH	…	7.2	7.2	7.2
Conductivity	µs/cm	12500	300	33000
Ca^{2+}	mg/L	720	10	2.08×10^3
Mg^{2+}	mg/L	335	5	0.77×10^3
Na^{+}	mg/L	1950	40	5.12×10^3
Cl^{-}	mg/L	3550	100	14.17×10^3
SO_4^{2-}	mg/L	2250	25	5.92×10^3
Fe^{3+}	mg/L	0.2	0.01	…
Ba^{2+}	ppb	10	…	…
Sr^{2+}	mg/L	13	…	…
HCO_3^{-}	mg/L	135	5	…
TDS	mg/L	9000	185	28000

The volume of treated raw water, permeate and rejected concentrate for the different lines are listed in Table 1.

In this study sample is taken from the D line (membrane-type polyamide). The compositions of the raw water and permeate are listed in Table 2.

3. Phase Diagram

Figure 1 shows the six-component system with reference tetrahedron, using Jänecke projection from the H_2O corner at 25 °C and 1 atm pressure and assuming halite saturation throughout. Any point in the interior of the tetrahedron represents a 6 component system and an invariant assemblage is formed by four salts + halite + solution. All field boundaries remain close to the bounding quinary triangles. Solubility calculations give brine compositions in equilibrium with a specified assemblage of minerals, and the evaporation of any water falling within the system can be followed quantitatively for equilibrium crystallization. In addition, the activities of all neutral species are known at every step. Furthermore, the effect of mixing brines or of adding salt minerals to given brine can be predicted.[14]

4. Experimental

In this work we study the reject brine from the reverse osmosis station of Skhira referred hereinafter by "Sk".

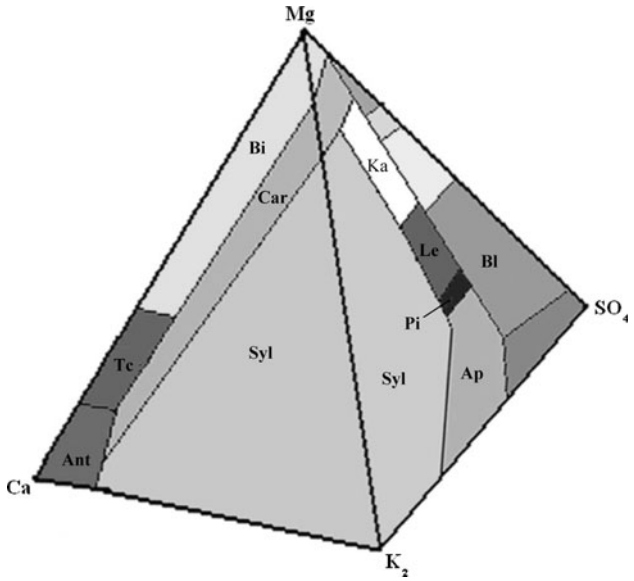

Fig. 1 Hexary system Na^+, Mg^{2+}, K^+, Ca^{2+}/Cl^-, $SO_4^{2-}//H_2O$

The brine undergoes an isothermal and isobaric evaporation (T = 25 °C) in order to follow its evolution during evaporation.

The evolution of evaporation is monitored daily. At each stage of evaporation specific gravity measurements was made and chemical analysis of liquid samples and different salts deposited are carried out. The recovered solids are also characterized by XRD and SEM.

4.1 Equipments and Analysis Methods

The equipment used for this work is listed below:

- A thermostatic bath fixed at 25 °C.
- A crystallizer for brine evaporation.
- A filtration equipment (a vacuum pump, a buchner and a vacuum flask).

The K^+ and Na^+ ions concentrations in the phases were analyzed by spectrophotometer using a Jenway PFP7 instrument. The Mg^{2+} and Ca^{2+} ions concentrations were determined by an EDTA complexometric titration. Potentiometric titration was applied to Cl^- ions (Titrino DMS 716, Ω Metrohm instrument). The SO_4^{2-} ion concentration was determined gravimetrically. The solid phases were often characterized by chemical analysis and XRD (the experimental apparatus is composed of a Philips PW 3040 generator, a PW 3050/60 θ/2θ goniometer and a PW 3373/00 copper cathode). The microstructural differences between the obtained salts were examined using ESM FEI Quanta 200.

5. Results and Discussion

The liquids and the precipitated salts were analyzed in order to determine the major ion composition of the brine,

and this analysis helped us to draw crystallization path on different diagrams. The precipitated solids recovered at each stage were analyzed by using x-ray diffractometry and Scanning electron microscopy. At the end a correlation between all these techniques was deduced in order to better evaluate these kinds of effluents.

5.1 Evolution of the Ionic Composition

In Fig. 2(a) and (b) it can be seen that the first regions begin at a specific gravity 1.0269 and ends at $d = 1.0313$; this area corresponds to a slight increase in the concentrations of Cl^-, SO_4^{2-}, Mg^{2+}, Na^+, K^+.

Between the specific gravity of 1.0313 and 1.194 there is a drop in the concentration of Ca^{2+}, and a significant increase in the concentrations of Na^+ and Cl^-, while concentrations of K^+, Mg^{2+}, and SO_4^{2-} increase slightly.

The observed variations can be attributed to the gypsum crystallization in this step and for a wide range of specific gravity [1.0313-1.1940].

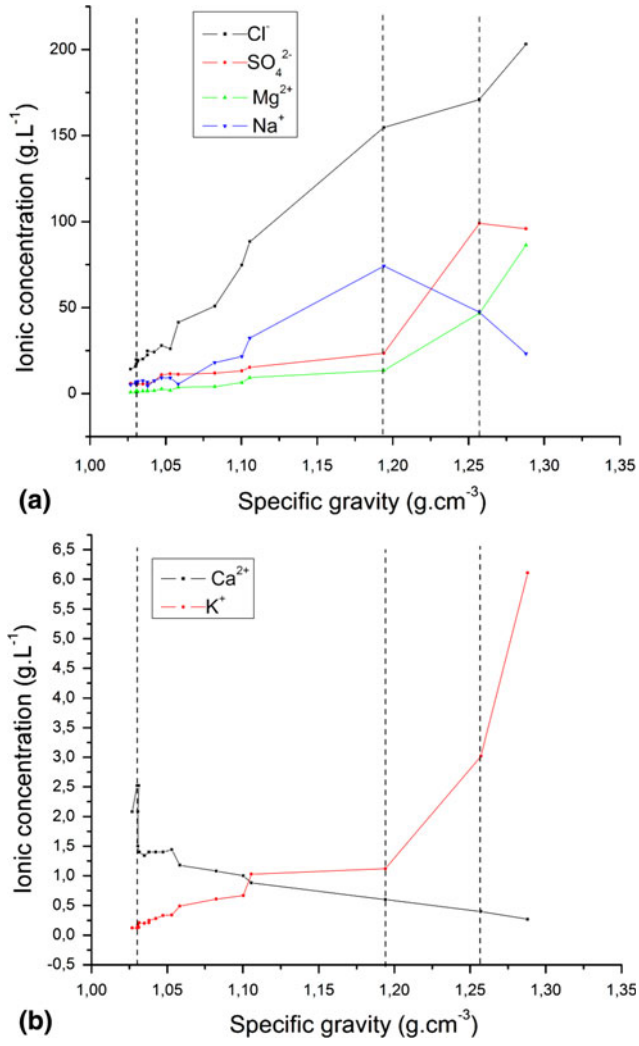

Fig. 2 (a) Evolution of ionic concentration of Na^+, Mg^{2+}, Cl^-, and SO_4^{2-} vs. specific gravity. (b) Evolution of ionic concentration of Ca^{2+} and K^+ vs. specific gravity

The decrease of Na^+ concentration is the most notable variation in the specific gravity interval [1.194-1.257]. The concentration of Cl^- is almost constant while the concentrations of Mg^{2+}, SO_4^{2-}, K^+ show an important increase. This variation is probably due to a crystallization of NaCl.

The last sequence [1.257-1.288] corresponds to:

- The concentration of Na^+ continuing to diminish.
- SO_4^{2-} concentration decreasing slightly.
- Concentrations of Mg^{2+}, Cl^-, and K^+ continuing to rise.

This change in composition is probably due to the crystallization of epsomite or the hexahydrite thereof.

5.2 Identification of the Recovered Salts by XRD

The characterization of deposited salts by XRD will make easier the identification of minerals nature corresponding to each sequence. Throughout this evaporation we have recovered 10 salts, the diffractograms of the four most representative salts are given by Fig. 3(a)-(d).

XRD confirms the deductions suggested by the evolution of ionic composition, in fact salt No. 1 is a pure gypsum (Fig. 3a), the salt No. 2 is constituted of halite + gypsum for the specific gravity range from 1.1065 to 1.194 (Fig. 3b). After this value is precipitated only NaCl (Fig. 3c), and the last sequence arises from a mixture of epsomite + hexahydrite + halite (Fig. 3d).

5.3 Morphological Characterization

We examined by SEM some salts among those characterized by XRD, this helped us to predict a correlation between morphological and mineralogical nature of recovered salts.

Figure 4(a) presents an image with a zoom 1200 times of salt No. 1, the texture of this salt is clear, showing needles of gypsum. In Fig. 4(b) we have the salt No. 3 enlarged 240 times; we note the presence of a cube with well-defined edges (NaCl). Figure 4(c) represents two photos of salt No. 4 with two enlargements, 800 times and 6000 times, with an prismatic shape very clearly characteristic of hexahydrite.

5.4 Crystallization Path

The crystallization path is the progress of physical transformations by the loss or the addition of a constituent through a given solubility phase diagram. During the system's evolution, it can define the number, the nature, the composition and the relative quantity of different condensed phases that precipitate or disappear. In our case, the constituent that disappears is the water, which leaves as water vapor at constant pressure and temperature. The graphic representation shows the reactions that occur by changing an intensive variable (pressure, temperature, composition).[15] Drawing the crystallization path demonstrates the extractive process from brines. If we adopt the Jänecke representation[11] from the bibliographic data compiled by d'Ans[12] to the representative point of the brine at 25 °C, we obtain a crystallization path in conformity with the Berthon rules.[13]

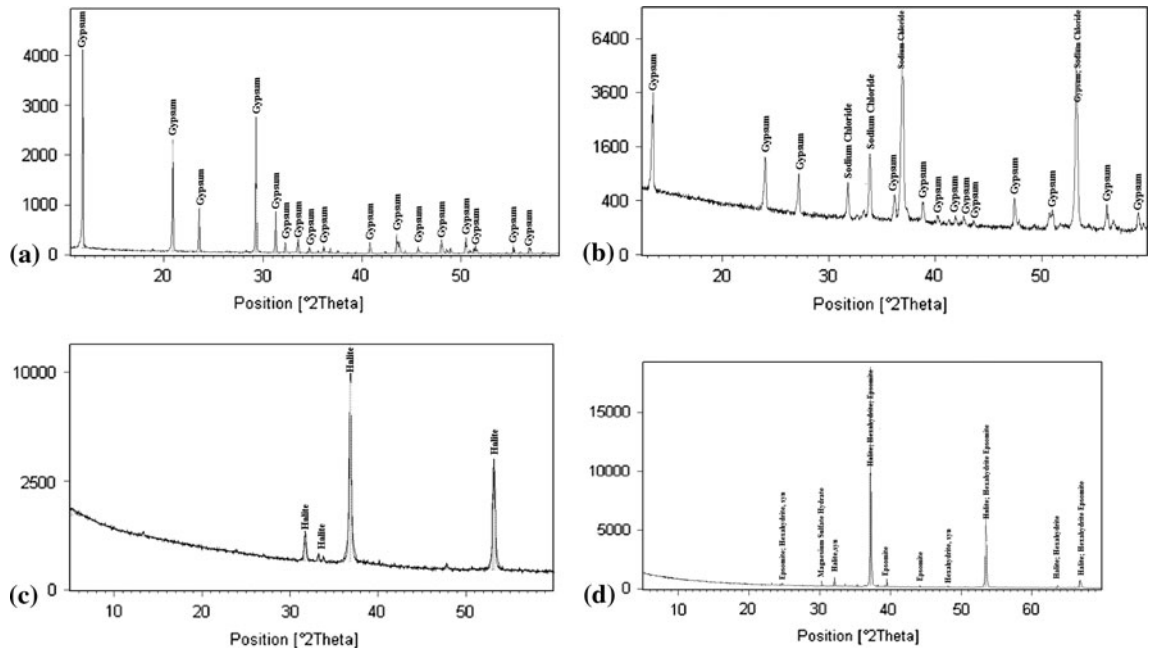

Fig. 3 (a) Diffractogram of salt No. 1, (b) diffractogram of salt No. 2, (c) diffractogram of salt No. 3, and (d) diffractogram of salt No. 4

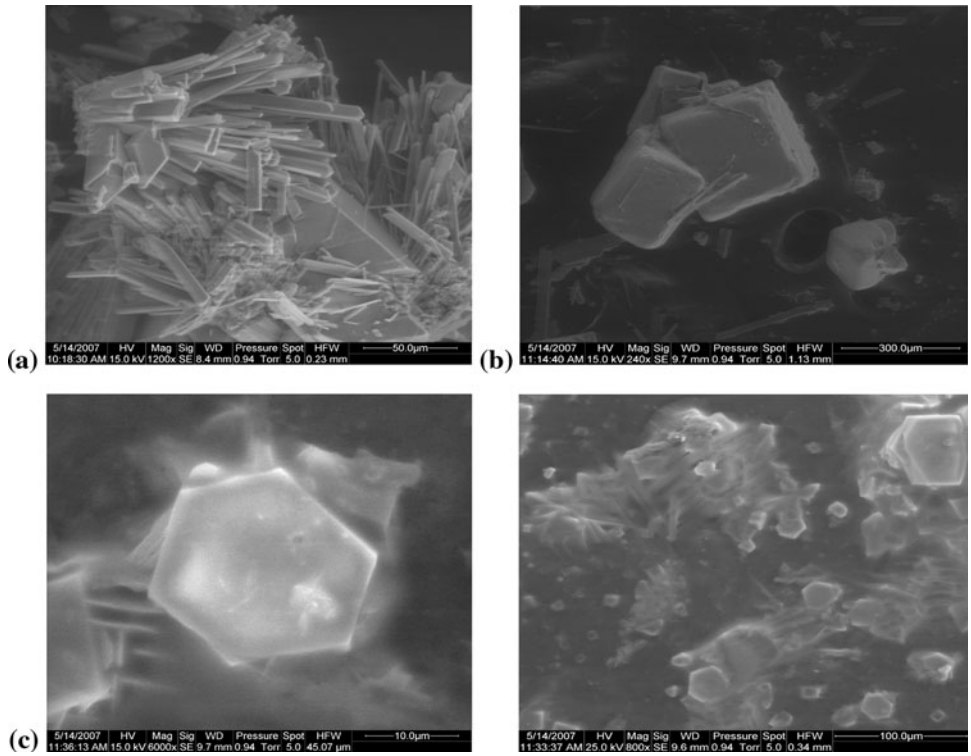

Fig. 4 (a) SEM image of salt No. 1, (b) SEM image of salt No. 3, and (c) SEM image of salt No. 4

Pratically and during evaporation, we filter the solution whenever the salts are deposited then we will remove salt deposits at every step of evaporation, and the crystallization path can cut the two salts line and continues until it reaches the border of a new line of two salts. Thus the crystallization path does not follow monovariant lines and there will be a

Table 3 Skhira concentrate composition (g/L)

Skhira concentrate	*d*	TDS	$[Cl^-]$	$[SO_4^{2-}]$	$[Mg^{2+}]$	$[Ca^{2+}]$	$[Na^+]$	$[K^+]$
	1.0269	28.06	14.17	5.926	0.77	2.08	5.118	0.12

Table 4 Coordinates of Skhira concentrate in the different systems

System	Coordinates of Skhira concentrate			
	$\%K_2$	%Ca	%Mg	$\%SO_4$
$Na^+, K^+, Mg^{2+}/Cl^-, SO_4^{2-}//H_2O$	1.61	…	33.37	65
$Na^+, K^+, Ca^{2+}/Cl^-, SO_4^{2-}//H_2O$	1.33	45	…	53.58
$Na^+, Mg^{2+}, Ca^{2+}/Cl^-, SO_4^{2-}//H_2O$	…	35.72	21.8	42.46
$Na^+, Mg^{2+}, K^+, Ca^{2+}/Cl^-, SO_4^{2-}//H_2O$	1.04	35.35	21.57	42.02

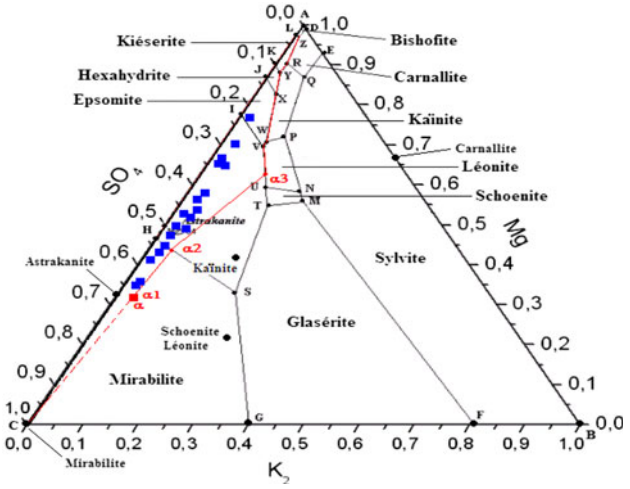

Fig. 5 Experimental and theoretical path for the system Na^+, K^+, Mg^{2+}/Cl^-, $SO_4^{2-}//H_2O$

change in the nature of the phase deposited when the figurative point arrive at a border. In Table 3 we have the ionic composition of the concentrate.

The crystallization paths were studied for the following quinary systems then for the hexary system:

$$Na^+,\ K^+, Mg^{2+}/Cl^-,\ SO_4^{2-}//H_2O$$

$$Na^+,\ K^+, Ca^{2+}/Cl^-,\ SO_4^{2-}//H_2O$$

$$Na^+,\ Mg^{2+}, Ca^{2+}/Cl^-,\ SO_4^{2-}//H_2O$$

The coordinates of the studied solutions in the different diagrams were calculated from the concentrations of the ions present in the brine and they are summarized in Table 4.

According to the figure, we note that the theoretical (line) and experimental (points) pathways evolve in the same direction. Theoretically, the crystallization point continues through Z.

While experimentally, it is limited to the field of epsomite. We notice that the salts recovered are different from those predictable in this diagram; this is explained that calcium is present in the brine but the adopted diagram ignores it (see Fig. 5).

This diagram shows in a very clear way that the theoretical and experimental paths are similar, also the points representing the brine are located in the area of anhydrite and the epsomite while theoretically it reach the point K3. It is also noted that the salts identified by XRD and those identified by crystallization paths are almost identical (see Fig. 6).

The experimental path follows a line up field thenardite, it is evolving in the same direction as the theoretical path to the areas rich in sulfate (see Fig. 7).

The application of hexary diagram to follow the path of the studied brine has been very beneficial because it gives us an opportunity to visualize the entire system without eliminating any constituent. In fact the initial solution starts from the anhydrite field until arriving at the domain of epsomite or hexahydrite with existence of halite in the majority of the process (see Fig. 8).

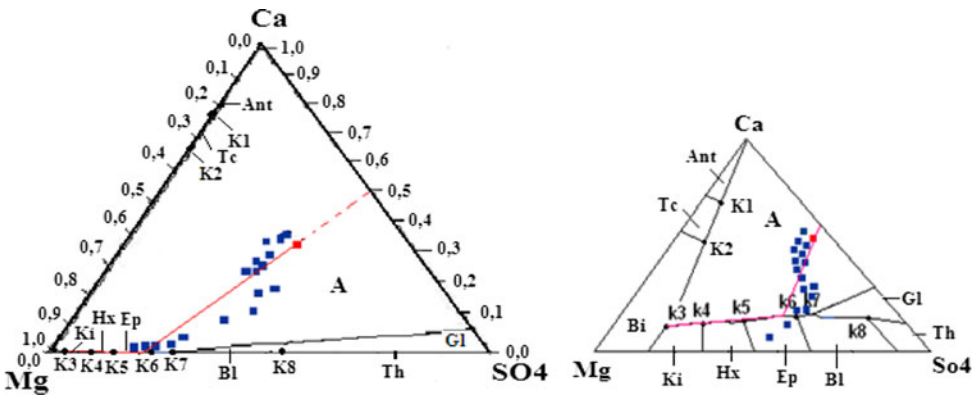

Fig. 6 Experimental and theoretical path for the system Na^+, Mg^{2+}, Ca^{2+}/Cl^-, $SO_4^{2-}//H_2O$

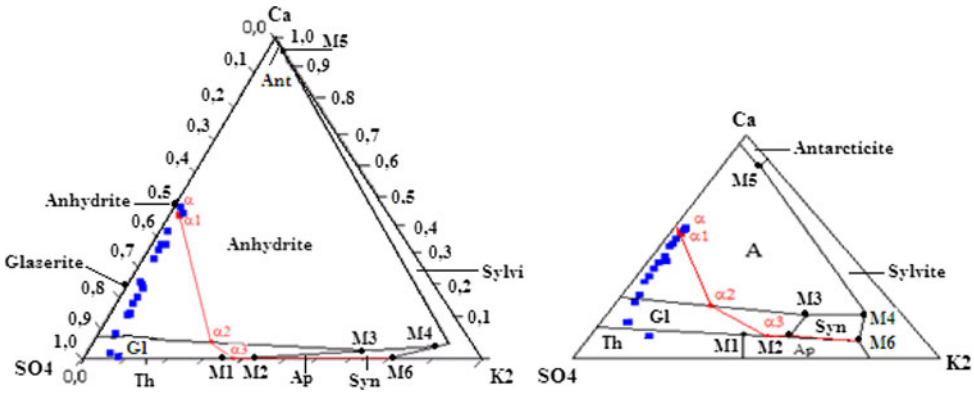

Fig. 7 Experimental and theoretical path for the system Na^+, K^+, Ca^{2+}/Cl^-, $SO_4^{2-}//H_2O$

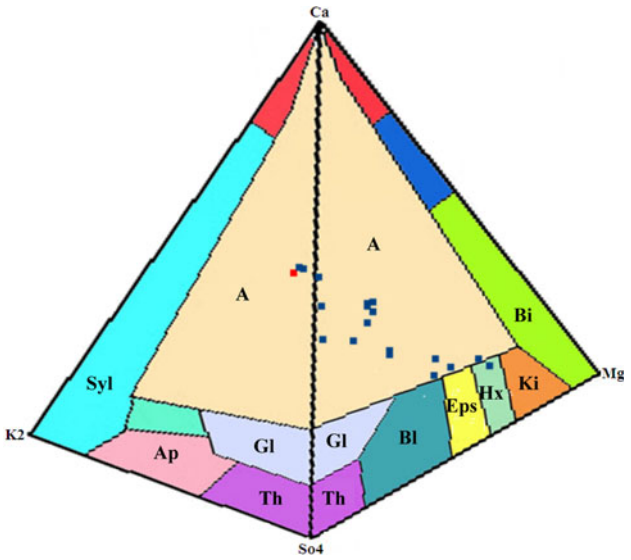

Fig. 8 Experimental and theoretical path for the system Na^+, Mg^{2+}, K^+, Ca^{2+}/Cl^-, $SO_4^{2-}//H_2O$

6. Conclusion

The comparison between experimental and predicted results shows good agreement due to the application of hexary diagram without changes in components. This will help us to navigate through the diagrams and to draw crystallization paths with the algebraic solution of material balances. Understanding the full scope of the studied diagram and the thermodynamics of the phase relationships is important for obtaining the most cost-effective process design in order to evaluate the reverse osmosis reject brines. In the future we plan to extend this study in a small scale pilot, so we can achieve the operation when the treatement of saline effluents will be considered as a resource recovery.

Acknowledgments

Authors would like to express their gratitude to all the people who have participated in this work. Part of the mentioned study was supported by the Tunisian Chemical Group (GCT). Finally we also wish to thank the technical team for helpful assistance with the XRD and SEM analysis.

References

1. M. Ahmed, A. Arakel, D. Hoey, M.R. Thumarukudy, M.F.A. Goosen, M. Al-Haddabi, and A. Al-Belushi, Feasibility of Salt Production from Inland RO Desalination Plant Reject Brine: A Case Study, *Desalination*, 2003, **158**, p 109-117
2. J.M. Arnal, M. Sancho, I. Iborra, J.M. Gozalvez, A. Santafe, and J. Lora, Concentration of Brines from RO Desalination Plants by Natural Evaporation, *Desalination*, 2005, **182**, p 435-439
3. H.K. Abdel-Aal, K.M. Ba-Lubaid, D.K. Al-Harbi, and A.A. Shaikh, Recovery of Mineral Salts and Potable Water from Desalting Plant Effluents by Evaporation. Part I. Evaluation of the Physical Properties of Highly Concentrated Brines, *Separation Sci. Technol.*, 1990, **25**(3), p 309-321
4. H.K. Abdel-Aal, K.M. Ba-Lubaid, A.A. Shaikh, and D.K. Al-Harbi, Recovery of Mineral Salts and Potable Water from Desalting Plant Effluents by Evaporation. Part II. Proposed Simulation System for Salt Recovery, *Separation Sci. Technol.*, 1990, **25**(4), p 437-461
5. Ö. Kilic and A.M. Kilic, Recovery of Salt Co-Products During the Salt Production from Brine, *Desalination*, 2005, **186**, p 11-19
6. M. Ahmed, W.H. Shayya, D. Hoey, A. Mahendran, R. Morris, and J. Al-Handaly, Use of Evaporation Ponds for Brine Disposal in Desalination Plants, *Desalination*, 2000, **130**, p 155-168
7. A.M.O. Mohamed, M. Maraqa, and J. Al Handhaly, Impact of Land Disposal of Reject Brine from Desalination Plants on Soil and Groundwater, *Desalination*, 2005, **182**, p 411-433
8. E. Gacia, O. Invers, M. Manzanera, E. Ballesteros, and J. Romero, Impact of the Brine from a Desalination Plant on a Shallow Seagrass (*Posidonia oceanica*) Meadow, *Estuar. Coastal Shelf Sci.*, 2007, **72**, p 579-590
9. I. Munoz and A.R. Fernandez-Alba, Reducing the Environmental Impacts of Reverse Osmosis Desalination by Using

Brackish Groundwater Resources, *Water Res.*, 2007, doi: 10.1016/j.watres.2007.08.021
10. T. Hoepner, A Procedure for Environmental Impact Assessments (EIA) for Seawater Desalination Plants, *Desalination*, 1999, **124**, p 1-12
11. E. Janecke, Ergänzung zu der neuen Darstellungsform der van't Hoffschen Untersuchungen, *Z. Anorg. Allgem. Chem.*, 1907, **53**, p 319
12. J. d'Ans, *Die Losungsgleichgewichte der Systeme der Salze Ozeanischer Salzablagerungen 2545 Kali-Forschung sanstalt*, Verl. ges. F. Ackerbau, 1933
13. R. Berthon, *Représentation des équilibres de solubilité et utilisation des diagrammes*, Gauthier-Villars, Paris, 1962, p 237-241
14. H.P. Eugster, C.E. Harvie, and J.H. Weare, Mineral Equilibria in a Six Component Seawater System, Na-K-Mg-Ca-SO_4-Cl-H_2O, at 25 °C, *Geochim. Cosmochim. Acta*, 1980, **44**, p 1335-1347
15. H. Hammi, J. Musso, A. M'nif, and R. Rokbani, Crystallization Path of a Natural Brine Evaporation Using the DPAO Method, *Desalination*, 2004, **166**, p 205-208